Phys Chem Minerals (2004) 31: 288–298
DOI 10.1007/s00269-004-0394-y

ORIGINAL PAPER

G. D. Gatta · T. Boffa Ballaran · P. Comodi
P. F. Zanazzi

Comparative compressibility and equation of state of orthorhombic and tetragonal edingtonite

Received: 19 November 2003 / Accepted: 25 February 2004

Abstract The high-pressure (H*P*) behaviour of a natural orthorhombic and tetragonal edingtonite from Ice River, Canada, has been investigated using in situ single-crystal X-ray diffraction. The two isothermal equations of state up to 6.74(5) GPa were determined. V_0, K_{T0} and K' refined with a third-order Birch–Murnaghan equation of state (BM-EoS) are: $V_0 = 598.70(7)$ Å^3, $K_{T0} = 59(1)$ GPa and $K' = 3.9(4)$ for orthorhombic edingtonite and $V_0 = 600.9(2)$ Å^3, $K_{T0} = 59(1)$ GPa and $K' = 4.2(5)$ for tetragonal edingtonite. The experiments were conducted with nominally hydrous pressure penetrating transmitting medium. No overhydration effect was observed within the pressure range investigated. At high-pressures the main deformation mechanism is represented by cooperative rotation of the secondary building unit (SBU).

Si/Al distribution slightly influences the elastic behaviour of the tetrahedral framework: the SBU bulk moduli are 125(8) GPa and 111(4) GPa for orthorhombic and tetragonal edingtonite, respectively. Extra-framework contents of both zeolites show an interesting behaviour under H*P* conditions: the split Ba2 site at $P > 2.85$ GPa is completely empty; only the position Ba1 is occupied.

Electronic Supplementary Material. Supplementary material to this paper (Observed and calculated structure factors) is available in electronic form at http://dx.doi.org/10.1007/s00269-004-0394-y.

G. D. Gatta (✉) · T. Boffa Ballaran
Bayerisches Geoinstitut, Universität Bayreuth,
Universität Str. 30, 95447 Bayreuth, Germany
e-mail: diego.gatta@uni-bayreuth.de

P. Comodi · P. F. Zanazzi
Dipartimento di Scienze della Terra,
Università di Perugia, Piazza Università 1,
06100 Perugia, Italy

Keywords Orthorhombic and tetragonal edingtonite · High-pressure single-crystal X-ray diffraction · Comparative compressibility

Introduction

Edingtonite ($Ba_2Al_4Si_6O_{20}\cdot 8H_2O$) is a "fibrous zeolite" (Gottardi and Galli 1985; Armbruster and Gunter 2001). The crystal structure was first determined by Taylor and Jackson (1933) in the $P\bar{4}2_1m$ space group. Two different structure types have been reported: orthorhombic ($P2_12_12$; Galli 1976; Kvick and Smith 1983; Gatta and Boffa Ballaran 2004) and tetragonal ($P\bar{4}2_1m$; Taylor and Jackson 1933; Mazzi et al. 1984; Gatta et al. 2004). The main difference between orthorhombic and tetragonal edingtonite is due to (Si,Al) disorder/order in the tetrahedra which reduces the lattice symmetry from $P\bar{4}2_1m$ to $P2_12_12$ (Fig. 1a). The framework of edingtonite consists of tetrahedral chains, running along [001] (Fig. 1b), built by the "4 = 1 secondary building unit (SBU)" (Baerlocher et al. 2001) with topological symmetry $P\bar{4}2_1m$ (Fig. 1a). The framework encloses two different systems of eight-membered ring channels: along [001] and along [110], in which lie the extra-framework cations and water molecules.

In edingtonite there is only one extra-framework cation site, preferentially occupied by Ba, and two independent water molecule sites. Mazzi et al. (1984) and Gatta and Boffa Ballaran (2004) showed that the Ba site can be split into two sites (Ba1 and Ba2), only 0.3–0.4 Å apart, in both tetragonal and orthorhombic edingtonite. In this case, most of the Ba cations (up to 90%) occupy the Ba1 site and a minor amount the Ba2 site. The coordination number of the Ba-polyhedron is 10: 6 framework oxygens and 4 water molecules.

Many studies have been dedicated to the high- and low-temperature behaviour of edingtonite (Van Reeuwijk 1972, 1974; Amitin et al. 1981; Belitsky et al.

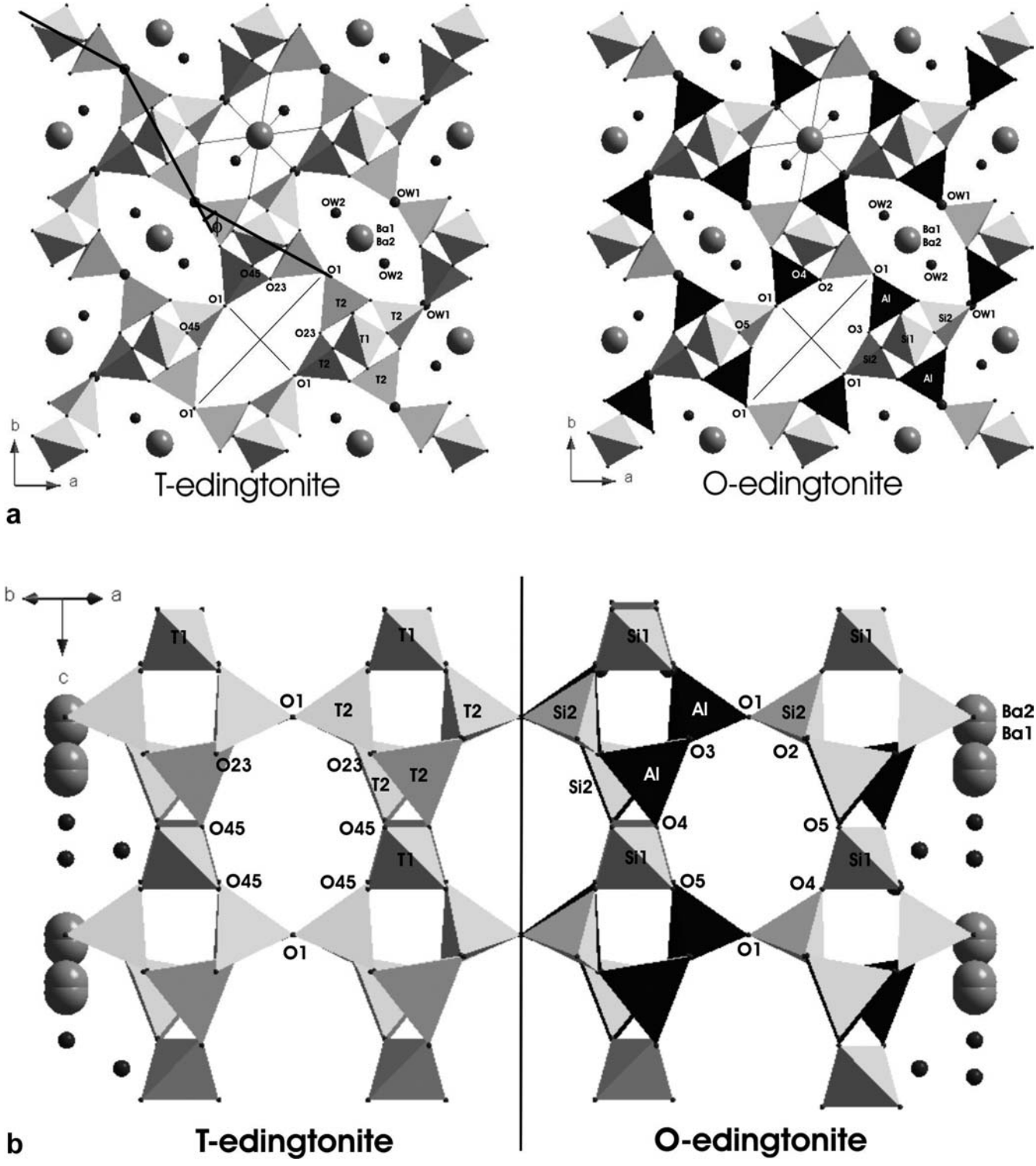

Fig. 1a,b Crystal structure of orthorhombic and of tetragonal edingtonite viewed **(a)** down [001] and **(b)** down [110]

1984, 1986, 1992; Goryainov and Belitsky 1986; Ståhl 1998; Ståhl and Hanson 1998; Goryainov et al. 2003). However, only two studies on the high-pressure structural evolution of edingtonite, supported by diffraction data, are reported in the literature: one done by single-crystal X-ray diffraction on tetragonal edingtonite with non-penetrating pressure-transmitting medium (Gatta et al. 2004) and the other using synchrotron X-ray powder diffraction with nominally penetrating pressure medium on orthorhombic edingtonite (Lee et al. 2004). A Raman study of edingtonite under high-pressure in a diamond anvil cell at room temperature was reported by Goryainov et al. (2003),

which shows that there is no pressure phase transition up to 6.4 GPa.

The bulk modulus values obtained by Gatta et al. (2004) and Lee et al. (2004) are sensibly different, K_{T0} = 57.9(6) GPa and K_{T0} = 73(3) GPa, respectively, and cannot be only due to the different experimental technique used. In order to clarify such different high-pressure behaviours, we investigated the structural behaviour of orthorhombic and tetragonal edingtonite under pressure by in situ X-ray single-crystal diffraction with nominally hydrous penetrating pressure-transmitting medium. This makes it possible to analyze the effects of the lattice microporosity on compressibility forcing water molecules to fill the channels.

The elastic behaviour and structural evolution of both specimens was also compared in order to analyze the role of the Si/Al distribution of the tetrahedral framework.

Experimental

The edingtonite sample came from the alkaline complex of Ice River, Canada. Both orthorhombic (O) and tetragonal (T) specimens occur in the same hydrothermal veins of the syenite. Since it is difficult to distinguish between the two specimens at the polarized light microscope, only X-ray diffraction of several single-crystals allowed the separation of the two crystal types. E. Galli from the University of Modena kindly provided crystals and chemical data of the T-edingtonite. The average unit-cell content is $(Ba_{1.82}\ Sr_{0.01}\ K_{0.11}\ Na_{0.03})(Al_{3.90}\ Si_{6.13})O_{20}{\cdot}7.30\ H_2O$. The chemical composition of orthorhombic edingtonite from the same locality (Ice River, Canada) was reported by Gatta and Boffa Ballaran (2004) and the resultant formula is: $(Ba_{1.96}\ K_{0.06}Na_{0.02})(Al_{3.95}Si_{6.35})O_{20}{\cdot}7.37\ H_2O$. Details on the microprobe and TG analysis for T- and O-edingtonite are reported in Mazzi et al. (1984) and Gatta and Boffa Ballaran (2004), respectively. Both chemical analyses refer to crystals of the same specimen (about 0.5 cm^3) from which the single crystals used in this experiment were extracted.

A Bayerisches Geoinstitut Diamond-Anvil Cell (DAC) (Allan et al. 1996) was used for the high-pressure experiments. Steel T301 foil, 250 μm thick with a 350-μm hole obtained by electrospark erosion, was used as a gasket. The gasket foil was pre-indented to a thickness of 110 μm before drilling the hole.

Two platy crystals, of O- and T-edingtonite, were placed together in the same gasket hole. A methanol:ethanol:water (16:3:1) mixture was used as nominally hydrous penetrating pressure-transmitting medium (Miletich et al. 2000). Ruby chips were used for pressure calibration according to Mao et al. (1986). The deviations in the measured pressure were less than ± 0.05 GPa.

Accurate lattice parameters were determined at T = 293 K and at pressures ranging between 0.0001 and 6.74 GPa (Table 1) at the Bayerisches Geoinstitut University of Bayreuth, by diffraction on a Huber SMC 9000 four-circle diffractometer (non-monochromatized Mo-$K\alpha$ radiation) using eight-position centring of 24 Bragg reflections (King and Finger 1979; Angel et al. 2000). Centring procedure and vector-least-squares refinement of the unit-cell parameters were performed by SINGLE software (Ralph and Finger 1982; Angel et al. 2000). Intensity data were collected in the range $2° \le 2\theta \le 60°$ with a Nonius-CAD4 diffractometer (graphite-monochromated Mo-$K\alpha$ radiation), operated at 50 kV and 40 mA, at 0.0001 GPa (crystal in DAC without pressure medium), 2.85 and 5.52 GPa. Details relative to the data collection are reported in Table 2.

Integrated intensity data were obtained processing the diffraction data using WinIntegrSTP3.4 computer program (Angel 2003a, b). Correction for Lorentz, polarization and absorption effects, for crystal and pressure cell, was applied using ABSORB5.2 computer program (Burnham 1966; Angel 2002). Absorption correction sensibly improved the quality of the diffraction data.

Finally, least-squares refinements were made with the SHELX-97 package (Sheldrick 1997). The structural refinements were conducted with isotropic thermal displacement factors starting from the coordinates of Gatta and Boffa Ballaran (2004) and Mazzi et al. (1984) for orthorhombic and tetragonal edingtonite respectively.

Only in the final least-squares cycles of the refinements was the Ba1 site refined with anisotropic displacement factors fixing the previously obtained occupancy factor; the lower occupied Ba2 was refined isotropically. This procedure was applied since the variance–covariance matrix showed a large correlation between barium occupancy factors and anisotropic thermal parameters. A similar refinement strategy was applied for all refinements of both zeolites.

Hydrogen atoms were not included, because they could not be found in the high–pressure refinements.

Neutral atomic scattering factor values of Si, Al, O and Ba, from the International Tables for X-ray Crystallography (Ibers and Hamilton 1974) were used. A structure refinement performed using ionic scattering curves yielded similar results. Since the two crystal structures are non-centrosymmetric, racemic/merohedral twinning by the pseudo-centre of symmetry and the correct choice of the "absolute structure" (correct, inverse) were considered in the

Table 1 Lattice parameters of (a) orthorhombic and (b) tetragonal edingtonite at different pressures

a)

P (GPa)	a (Å)	b (Å)	c (Å)	V (Å)^3
0.0001	9.5342(6)	9.6445(7)	6.5110(7)	598.70(7)
0.81(5)	9.4991(7)	9.5996(10)	6.4866(7)	591.50(8)
1.24(5)	9.4696(6)	9.5719(6)	6.4742(7)	586.84(6)
1.62(5)	9.4494(5)	9.5517(5)	6.4654(6)	583.56(6)
2.18(5)	9.4175(6)	9.5189(7)	6.4519(6)	578.38(6)
2.85(5)	9.3804(6)	9.4839(6)	6.4354(6)	572.51(6)
3.30(5)	9.3595(4)	9.4643(4)	6.4253(4)	569.16(4)
4.25(5)	9.3168(5)	9.4215(6)	6.4044(5)	562.17(5)
4.63(5)	9.2996(8)	9.4063(8)	6.3956(9)	559.46(8)
5.52(5)	9.2612(6)	9.3680(7)	6.3744(7)	553.03(6)
6.00(5)	9.2425(5)	9.3509(5)	6.3636(6)	549.97(5)
6.74(5)	9.2106(4)	9.3210(5)	6.3438(6)	544.63(5)
5.15(5)[a]	9.2770(6)	9.3836(7)	6.3841(6)	555.75(6)
3.54(5)[a]	9.3515(7)	9.4546(8)	6.4205(6)	567.67(6)
1.70(5)[a]	9.4482(6)	9.5487(7)	6.4648(6)	583.24(5)
0.77(5)[a]	9.5041(6)	9.6045(9)	6.4880(4)	592.24(6)

b)

P (GPa)	a (Å)	c (Å)	V (Å)^3
0.0001	9.5911(11)	6.5315(17)	600.83(21)
0.81(5)	9.5503(10)	6.5088(15)	593.66(19)
1.24(5)	9.5213(9)	6.4958(14)	588.87(17)
1.62(5)	9.5007(10)	6.4880(16)	585.63(18)
2.18(5)	9.4677(9)	6.4744(14)	580.38(17)
2.85(5)	9.4308(9)	6.4604(12)	574.60(15)
3.30(5)	9.4089(9)	6.4514(13)	571.14(16)
4.25(5)	9.3644(9)	6.4328(12)	564.10(15)
4.63(5)	9.3466(8)	6.4258(12)	561.35(14)
5.52(5)	9.3080(8)	6.4079(11)	555.17(13)
6.00(5)	9.2872(8)	6.3978(12)	551.82(14)
6.74(5)	9.2567(9)	6.3818(13)	546.84(14)
5.15(5)[a]	9.3245(8)	6.4155(11)	557.81(13)
3.54(5)[a]	9.3999(8)	6.4483(12)	569.77(15)
1.70(5)[a]	9.4991(12)	6.4868(15)	585.32(20)
0.77(5)[a]	9.5536(13)	6.5096(16)	594.13(23)

[a] Data collected during decompression

Table 2 Details of data collection and structural refinements of (a) orthorhombic and (b) tetragonal edingtonite at different pressures Note: The low number of the total reflections measured at 2.85 GPa for the T-edingtonite was due to some technical problems. The data collection was not completed, but the few reflections (*n*. 202) were collected within the range $2° < 2\theta < 60°$

a)

Pressure (GPa)	0.0001[a]	2.85(5)	5.52(5)
Crystal size (μm^3)	170 × 90 × 60	170 × 90 × 60	170 × 90 × 60
Radiation	Mo*Kα*	Mo*Kα*	Mo*Kα*
2θ range (°)	2–60	2–60	2–60
Scan type	ω	ω	ω
Scan speed (°/min)	2.06	2.06	2.06
Scan width (°)	0.8	0.8	0.8
Space group	$P\,2_12_12$	$P\,2_12_12$	$P\,2_12_12$
Reflections measured	879	848	856
Unique refl. (total)	746	737	721
Unique refl. with $F_o > 4\sigma(F_o)$	392	415	378
Parameters refined	49	47	47
R_{int}[b]	0.031	0.031	0.059
R_1 (F)[c]	0.035	0.037	0.043

b)

Pressure (GPa)	0.0001[a]	2.85(5)	5.52(5)
Crystal size (μm^3)	180 × 100 × 70	180 × 100 × 70	180 × 100 × 70
Radiation	Mo*Kα*	Mo*Kα*	Mo*Kα*
2θ range (°)	2–60	2–60	2–60
Scan type	ω	ω	ω
Scan speed (°/min)	2.06	2.06	2.06
Scan width (°)	0.8	0.8	0.8
Space group	$P\,\bar{4}\,2_1m$	$P\,\bar{4}\,2_1m$	$P\,\bar{4}\,2_1m$
Reflections measured	854	202	1067
Unique refl. (total)	559	103	565
Unique refl. with $F_o > 4\sigma(F_o)$	292	92	305
Parameters refined	31	28	28
R_{int}[b]	0.092	0.045	0.045
R_1 (F)[c]	0.046	0.037	0.037

[a] data collected under room conditions with crystal in the DAC without pressure medium

[b] $R_{int} = \Sigma|\,Fobs^2 - Fobs^2(mean)\,|/\Sigma[\,Fobs^2\,]$

[c] $R_1(F) = \Sigma(|Fobs|-|Fcalc|)/\Sigma|Fobs|$

structural refinements according to the Flack test (Flack 1983). The Flack test confirmed a correct structure choice and the absence of racemic twinning for both zeolites. Results from the refinements are listed in Tables 3, 4 and 5. Observed and calculated structure factors can be obtained from the authors upon request (or through the Editorial Office).

Results

Comparative compressibility

High-pressure unit-cell parameters of orthorhombic and tetragonal edingtonite in the investigated pressure range (from 0.0001 to 6.74 GPa) are summarized in Table 1. The changes in the lattice parameters with pressure, normalized with respect to the room condition value, are shown in Fig. 2. No phase transition was observed within the pressure range investigated. Despite the nominally penetrating hydrous pressure medium used in this experiment, no overhydration effect was observed, as indicated by the continuous cell-parameter variations. Also to compare the lattice parameter results, the evolution of the cell volume with pressure for both zeolites is shown in Fig. 3.

Volume finite strain – stress plots (*fe–Fe* plot; Angel 2000) are shown in Fig. 4. The weighted linear regressions through the volume data points yield practically horizontal trends for both specimens, indicating that the bulk modulus (K_{T0}) of the two specimens is similar and that its pressure derivative (K') is very close to 4.

P–V data were fitted with a third-order Birch–Murnaghan equation-of-state (BM-EoS) (Birch 1947), with EOS-FIT5.2 computer program (Angel 2001). The EoS parameters obtained, using the weighted data by the uncertainties in *P–V*, are: $V_0 = 598.70(7)$ Å^3, $K_{T0} = 59(1)$ GPa, $K' = 3.9(4)$ for O-edingtonite and $V_0 = 600.9(2)$ Å^3, $K_{T0} = 59(1)$ GPa, $K' = 4.2(5)$ for T-edingtonite. The K' values are approximately 4, in good agreement with the horizontal line fitting the volume *fe–Fe* data for both zeolites (Fig. 4). Therefore the H*P*-behaviour of edingtonites could be adequately described by a second-order BM-EoS (Angel 2000): $V_0 = 598.71(7)$ Å^3 and $K_{T0} = 59.3(2)$ GPa for O-edingtonite, $V_0 = 600.9(2)$ Å^3 and $K_{T0} = 59.3(4)$ GPa for T-edingtonite.

The "axial bulk moduli" were calculated with "linearized" BM-EoS (Angel 2000), simply by substituting the cube of the individual lattice parameter (a^3, b^3, c^3) for the volume. The elastic parameters of O-edingtonite obtained using a third-order BM-EoS are: $a_0 = 9.5346(9)$ Å, $K_{T0a} = 55(1)$ GPa and $K'_a = 3.1(5)$ for the *a*-axis; $b_0 = 9.6447(8)$ Å, $K_{T0b} = 50(1)$ GPa and $K'_b = 5.2(4)$ for the *b*-axis; $c_0 = 6.5101(9)$ Å, $K_{T0c} = 79(2)$ GPa and $K'_c = 2.9(8)$ for the *c*-axis ($K_{T0a} : K_{T0b} : K_{T0c} = 1.1:1.0:1.6$). For the tetragonal specimens we obtain: $a_0 = 9.592(1)$ Å, $K_{T0a} = 52(1)$ GPa and $K'_a = 3.6(4)$ for the *a*-axis; $c_0 = 6.529(1)$ Å, $K_{T0c} = 82(4)$ GPa and $K'_c = 6(1)$ for the *c*-axis ($K_{T0a} : K_{T0b} : K_{T0c} = 1.0:1.0:1.6$).

An increase in the full-width-at-half-maximum of the diffraction peaks at pressures higher than 6 GPa, probably due to the first steps of collapsing of the crystal structure, prevented the centring procedure and the accurate lattice-parameter determination. However, the diffraction data collected during decompression show that the structural modifications induced up to 6.5 GPa are reversible (Fig. 2, Table 1).

Crystal structure under room conditions

The crystal structures of orthorhombic and tetragonal edingtonite were refined at room pressure from the data collected with the crystals in the DAC without pressure medium. The cell parameters and the refined atomic positions of the framework and extra-framework

Table 3 Atomic position and thermal displacement parameters (Å^2) for (a) orthorhombic and (b) tetragonal edingtonite at different pressures. Note: For each atom, values from top to bottom correspond to the refinement at 0.0001 GPa in the DAC, 2.85(5) and 5.52(5) GPa, respectively. For the *Ba1* site the anisotropic thermal parameters, *Ueq*, is reported, whereas for the other sites the isotropic displacement parameter, *Uiso*, is shown

a)

Site	*x*	*y*	*z*	Site occupancy	*U*iso/*U*eq
Ba1	0.5	0.0	0.63529(36)	0.86(2)	0.01455(39)
	0.5	0.0	0.63760(14)	1.01(1)	0.01150(34)
	0.5	0.0	0.64043(18)	0.98(2)	0.01226(42)
Ba2	0.5	0.0	0.5848(20)	0.12(2)	0.0110(38)
	–	–	–	–	–
	–	–	–	–	–
Si1	0.0	0.0	0.01344(52)	1.0	0.00873(77)
	0.0	0.0	0.01059(56)	1.0	0.00685(79)
	0.0	0.0	0.00867(77)	1.0	0.0113(10)
Si2	−0.17601(28)	0.09285(34)	0.38782(47)	1.0	0.00684(62)
	−0.17994(34)	0.09045(42)	0.38505(51)	1.0	0.00537(67)
	−0.18216(45)	0.08943(59)	0.38426(68)	1.0	0.00988(91)
Al	0.09164(30)	0.17163(35)	0.62672(58)	1.0	0.00657(62)
	0.08786(37)	0.17553(41)	0.62465(59)	1.0	0.00544(71)
	0.08523(48)	0.17802(54)	0.62339(81)	1.0	0.00781(94)
O1	0.17395(76)	0.33032(90)	0.6311(14)	1.0	0.0113(15)
	0.16583(90)	0.3383(10)	0.6404(15)	1.0	0.0102(17)
	0.1602(11)	0.3443(13)	0.6440(20)	1.0	0.0116(22)
O2	−0.05306(77)	0.1973(11)	0.4672(12)	1.0	0.0093(19)
	−0.0561(10)	0.1996(14)	0.4575(14)	1.0	0.0138(23)
	−0.0585(13)	0.2022(18)	0.4514(19)	1.0	0.0164(29)
O3	0.19845(90)	0.03874(90)	0.5375(11)	1.0	0.0120(20)
	0.1959(12)	0.0397(11)	0.5442(13)	1.0	0.0123(22)
	0.1976(16)	0.0421(13)	0.5465(17)	1.0	0.0129(29)
O4	0.03667(65)	0.13475(93)	0.8749(13)	1.0	0.0104(18)
	0.02511(98)	0.1368(12)	0.8750(13)	1.0	0.0158(22)
	0.0202(13)	0.1411(14)	0.8736(17)	1.0	0.0146(26)
O5	−0.13484(80)	0.03685(81)	0.1577(11)	1.0	0.0112(20)
	−0.13933(92)	0.0264(11)	0.1552(12)	1.0	0.0124(21)
	−0.1420(11)	0.0164(18)	0.1535(16)	1.0	0.0166(24)
OW1	0.1749(13)	0.3245(15)	0.1485(22)	0.94(3)	0.0432(44)
	0.1804(13)	0.3171(15)	0.1631(17)	1.00(4)	0.0272(39)
	0.1852(17)	0.3127(19)	0.1702(23)	1.00(5)	0.0310(54)
OW2	0.3789(15)	0.1227(18)	−0.0192(21)	1.00(4)	0.0622(60)
	0.3813(16)	0.1178(20)	−0.0185(22)	1.00(5)	0.0485(56)
	0.3827(23)	0.1142(26)	−0.0141(31)	1.00(6)	0.0561(76)

b)

Site	*x*	*y*	*z*	Site occupancy	*U*iso/*U*eq
Ba1	0.5	0.0	0.64080(45)	0.88(1)	0.02083(54)
	0.5	0.0	0.64285(20)	0.92(2)	0.0209(23)
	0.5	0.0	0.64494(17)	0.96(1)	0.01361(34)
Ba2	0.5	0.0	0.5754(37)	0.08(2)	0.0203(79)
	–	–	–	–	–
	–	–	–	–	–
T1	0.0	0.0	0.0	1.0	0.0159(12)
	0.0	0.0	0.0	1.0	0.0182(38)
	0.0	0.0	0.0	1.0	0.01364(86)
T2	−0.17460(38)	0.09295(39)	0.38141(52)	1.0	0.01339(79)
	−0.1745(13)	0.0899(13)	0.38032(47)	1.0	0.0129(11)
	−0.18016(30)	0.08504(31)	0.38056(39)	1.0	0.01314(58)
O1	0.1723(11)	0.3276(11)	0.6188(21)	1.0	0.0185(28)
	0.1642(36)	0.3358(36)	0.6312(18)	1.0	0.0182(38)
	0.16095(84)	0.33905(84)	0.6319(17)	1.0	0.0187(21)
O23	−0.04415(98)	0.1957(12)	0.4650(13)	1.0	0.0202(23)
	−0.0503(23)	0.1907(24)	0.4566(12)	1.0	0.0146(28)
	−0.05078(75)	0.19593(93)	0.4534(10)	1.0	0.0153(16)
O45	−0.1392(10)	0.03753(91)	0.1444(15)	1.0	0.0197(21)
	−0.1467(25)	0.0301(30)	0.1430(11)	1.0	0.0162(24)
	−0.14537(81)	0.02023(89)	0.1436(11)	1.0	0.0222(15)
OW1	0.1749(16)	0.3251(16)	0.1446(32)	0.90(4)	0.0392(62)
	0.1819(41)	0.3181(41)	0.1569(24)	1.00[a]	0.0421(62)
	0.1849(10)	0.3151(10)	0.1651(19)	1.00[a]	0.0276(26)
OW2	0.3763(19)	0.1237(19)	−0.0183(32)	1.00[a]	0.0619(62)
	0.3776(28)	0.1224(28)	−0.0152(29)	1.00[a]	0.0599(88)
	0.3796(14)	0.1204(14)	−0.0162(24)	1.00[a]	0.0531(42)

[a] The occupancy factors were 1.00 within their esds and, to reduce the number of the refined parameters, were then fixed to 1.00

Table 4 Interatomic distances (Å) of (a) orthorhombic and (b) tetragonal edingtonite at different pressures

a)

P (GPa)	0.0001[a]	2.85(5)	5.52(5)
Ba1–O1 (x 2)	2.905(9)	2.823(9)	2.759(12)
Ba1–O2 (x2)	3.037(10)	2.961(13)	2.901(16)
Ba1–O3 (x2)	2.968(9)	2.939(11)	2.890(14)
Ba1–OW1 (x 2)	2.762(14)	2.742(13)	2.734(17)
Ba1–OW2 (x 2)	2.791(15)	2.718(15)	2.678(21)
Ba1–O1 (x 2)	2.721(11)	–	–
Ba1–O2 (x2)	2.982(10)	–	–
Ba1–O3 (x2)	2.915(9)	–	–
Ba1–OW1 (x 2)	2.943(16)	–	–
Ba1–OW2 (x 2)	3.062(19)	–	–
Si1–O4 (x 2)	1.620(9)	1.581(11)	1.589(12)
Si1–O5 (x 2)	1.631(8)	1.624(8)	1.614(11)
< Si1–O >	1.625	1.602	1.601
Si2–O1	1.616(8)	1.605(9)	1.596(11)
Si2–O2	1.629(9)	1.625(12)	1.616(16)
Si2–O3	1.614(9)	1.611(10)	1.615(13)
Si2–O5	1.641(8)	1.644(9)	1.664(13)
< Si2–O >	1.625	1.621	1.623
Al–O1	1.720(9)	1.711(10)	1.711(13)
Al–O2	1.744(8)	1.741(10)	1.739(13)
Al–O3	1.737(9)	1.719(11)	1.716(14)
Al–O4	1.736(9)	1.754(9)	1.739(12)
< Al–O >	1.734	1.731	1.726

b)

P (GPa)	0.0001[a]	2.85(5)	5.52(5)
Ba1–O1 (x 2)	2.888(14)	2.816(38)	2.763(11)
Ba1–O23 (x4)	3.029(11)	3.025(23)	2.938(8)
Ba1–OW1 (x 2)	2.755(22)	2.749(50)	2.721(13)
Ba1–OW2 (x 2)	2.787(22)	2.747(27)	2.688(16)
Ba2–O1 (x 2)	2.659(19)	–	–
Ba2–O23 (x 4)	2.961(12)	–	–
Ba2–OW1 (x 2)	2.995(26)	–	–
Ba2–OW2 (x 2)	3.139(30)	–	–
T1–O45 (x 4)	1.674(9)	1.688(21)	1.647(7)
T2–O1	1.654(6)	1.677(20)	1.641(4)
T2–O23	1.666(10)	1.586(28)	1.653(8)
T2–O23'	1.683(11)	1.698(22)	1.659(7)
T2–O45	1.672(10)	1.654(14)	1.666(7)
< T2–O >	1.669	1.654	1.655

[a] Data collected at room conditions with crystal in the DAC without pressure medium

content (Tables 1, 3) are in good agreement with those found for the refinements of O- and T-edingtonite from Ice River (Canada) (Mazzi et al. 1984; Gatta and Boffa Ballaran 2004) with the crystals in air.

Special care was taken to locate the split Ba site (Ba1, Ba2) and of the oxygens of water molecules (OW1, OW2). In particular, in O-edingtonite the Ba^{2+} site is split into two sites $\sim$ 0.33 Å apart. The occupancy factor of Ba1 and Ba2 sites are $\sim$ 86% and $\sim$ 12%, respectively (Table 3a), whereas the occupancies of the water molecule sites OW1 and OW2 are $\sim$ 94% and $\sim$ 100%, respectively. Al and Si are fully ordered into Al, Si1 and Si2 sites, as confirmed by Al–O, Si1–O and Si2–O mean bond distances, which are 1.734, 1.625 and 1.625 Å, respectively (Table 4a). The Si/Al ordering in the tetrahedral framework demonstrates the effective general orthorhombic symmetry of this specimen.

In T-edingtonite the Ba^{2+} site is split into two sites $\sim$ 0.43 Å apart, and the occupancy factor of Ba1 and Ba2 sites is $\sim$ 88% and $\sim$ 8% respectively (Table 3b). The sum of the occupancy factors of the two sites is lower than 100%. The occupancies of the water molecule sites are $\sim$ 90% for OW1 and $\sim$ 100% for OW2. The tetrahedral bond distances demonstrate the effective Si/Al disordering in the tetrahedral framework and confirm the real general tetragonal symmetry of this specimen. T1–O and T2–O bond distances are reported in Table 4b.

H*P*-crystal structures

Two structural refinements under H*P*-conditions (2.85 and 5.52 GPa) were carried out. The main deformation mechanism occurs in the polyhedral tilting that produces intertetrahedral angle variations without any relevant variations in the tetrahedral bond distances (Tables 4, 5). A cooperative rotation (antirotation) of the SBU along [001] leads to the most relevant structural variations (Fig. 5), and the SBU would be considered, at a first approximation, as a rigid unit. A similar mechanism was observed by Comodi et al. (2002) and Ballone et al. (2002) for scolecite (Ca-fibrous zeolite).

The SBU-antirotation mechanism modifies the channel geometry. We analysed the ellipticity variation as a consequence of applied pressure. The ellipticity coefficients (ε), here defined as the ratio smaller/larger "free diameters" (Baerlocher et al. 2001), are strongly modified with increasing pressure. In O-edingtonite, $\varepsilon_{[001]}$ = O1↔O1(short)/O1↔O1(long) changes from 0.32, at ambient pressure, to 0.23 at 5.52 GPa (–28%), whereas $\varepsilon_{[110]}$ = O4↔O5(long)/O1↔O1 from 0.72 (*P* = 0.0001 GPa) to 0.62 at 5.52 GPa (–14%) (Table 5a). In T-edingtonite, for the same pressure range, $\varepsilon_{[001]}$ changes from 0.32 to 0.25 (–22%), whereas $\varepsilon_{[110]}$ (in this case O45↔O45(long)/O1↔O1) from 0.70 to 0.60 (–14%) (Table 5b). The increase in ellipticity is correlated with the angle variation between the eight-tetrahedra-membered rings. In O-edingtonite, in the pressure range from 0.0001 to 5.52 GPa, the obtuse angle of the [001] channel, (O4-O1-O5)°, increases from 111.00(8)° to 114.82(11)°; the acute angle, (O2-O1-O3)°, decreases from 77.02(8)° to 71.46(8)° (Table 5a). The angle between the [001] chains, shown in Fig. 1a and defined as $\varphi° = [180°-(O1–O1–O1)°]/2$, increases from 17.37(6)° to 20.22(8)° (Table 5a). Similar behaviour is also observed for the tetragonal specimen: (O45–O1–O45)° increases from 108.14(11)° to 112.16(11)° whereas (O23–O1–O23)° decreases from 78.70(8)° to 74.39(9)°, $\varphi° = [180°-(O1–O1–O1)°]/2$ changes from 17.30(7)° to 19.60(8)° (Table 5b).

To investigate the effect of the Si/Al distribution on the elastic behaviour of the tetrahedral framework, the

Table 5 Selected structural parameters for (a) orthorhombic and (b) tetragonal edingtonite at different pressures

a)

P (GPa)	0.0001[a]	2.85(5)	5.52(5)	K_{T0} (GPa)
Vol– "Prismatic SBU" (Å^3)	164.30(5)	160.15(7)	156.99(7)	125(8)
Si1–Si1 (Å)	6.511(4)	6.435(7)	6.374(6)	
Si2–Si2 (Å)	3.804(5)	3.787(8)	3.767(7)	
Al–Al (Å)	3.743(4)	3.715(7)	3.690(6)	
Si1–O5–Si2(°)	141.83(7)	139.40(11)	136.59(9)	
Si1–O4–Al (°)	138.41(9)	136.77(12)	134.66(10)	
φ(°)	17.37(6)	19.03(5)	20.22(8)	
Channel [001]				
O1↔O1 (Å)	1.960(4)	1.668(6)	1.460(7)	
("free diameter")				
O1↔O1 (Å)	6.202(5)	6.271(8)	6.313(8)	
O3↔O2 (Å)	0.778(4)	0.694(5)	0.592(7)	
O2–O1–O3 (°)	77.02(8)	74.21(7)	71.46(8)	
O4–O1–O5 (°)	111.00(8)	113.64(9)	114.82(11)	
$\varepsilon_{[001]}$[b]	0.32	0.27	0.23	
Channel [110]				
O1↔O1 (Å)	3.811(4)	3.735(6)	3.674(8)	
O2↔O3 (Å)	2.020(6)	1.971(6)	1.916(8)	
O2↔O3 (Å)	0.778(3)	0.694(5)	0.592(8)	
O4↔O5 (Å)	1.759(3)	1.789(7)	1.784(7)	
O4↔O5 (Å)	2.755(5)	2.476(7)	2.265(9)	
$\varepsilon_{[110]}$[b]	0.72	0.66	0.62	

b)

P (GPa)	0.0001[a]	2.85(5)	5.52(5)	K_{T0} (GPa)
Vol–"Prismatic SBU" (Å^3)	164.66 (4)	160.58(6)	156.41(7)	111(4)
T1–T1 (Å)	6.531(5)	6.460(8)	6.408(7)	
T2–T2 (Å)	3.794(4)	3.702(6)	3.709(8)	
T1–O45–T2(°)	138.76(6)	133.96(8)	135.27(11)	
φ(°)	17.30(7)	18.94(9)	19.60(8)	
Channel [001]				
O1↔O1 (Å)	1.975(6)	1.679(8)	1.537(6)	
("free diameter")				
O1↔O1 (Å)	6.188(5)	6.258(9)	6.226(8)	
O23↔O23 (Å)	0.829(5)	0.755(6)	0.634(8)	
O23–O1–O23 (°)	78.70(8)	77.39(7)	74.39(9)	
O45–O1–O45 (°)	108.14(11)	110.17(12)	112.16(11)	
$\varepsilon_{[001]}$[b]	0.32	0.27	0.25	
Channel [110]				
O1↔O1 (Å)	3.831(7)	3.760(7)	3.708(9)	
O23↔O23 (Å)	2.027(6)	2.096(8)	1.971(7)	
O23↔O23 (Å)	0.829(4)	0.755(6)	0.634(7)	
O45↔O45 (Å)	2.702(5)	2.413(8)	2.234(6)	
O45↔O45 (Å)	1.684(6)	1.610(5)	1.702(6)	
$\varepsilon_{[110]}$[b]	0.70	0.64	0.60	

[a] Data collected under room conditions with crystal in DAC without pressure medium

[b] esds values are less than 0.005

SBU bulk moduli for both zeolites have been calculated. SBU volumes at different pressure values were calculated considering the building unit as a prism with rhombic section, delimited by the four oxygen atoms (O1), and with height represented by the distances between T1–T1 (or Si1–Si1) tetrahedra (Table 5). The SBU is completely inscribed in this polyhedron. The two SBU bulk moduli, calculated from a weighted linear regression, are 125(8) and 111(4) GPa for O- and T-edingtonite respectively.

Special care was devoted to analyze the extraframework content behaviour at high pressure. The structural refinements of both specimens show that the occupancy of the Ba1 and Ba2 sites changes with pressure. At 2.85 GPa the Ba2 site is completely empty and only the position Ba1 is occupied (Table 3). A similar effect was observed by Gatta et al. (2004) for tetragonal edingtonite in a non-penetrating medium: at 2.28 GPa the occupancy factor of the Ba2 site is 0.04(4); we observe a completely empty Ba2 site at 2.85 GPa.

Despite the hydrous pressure medium used in this experiment, no evidence of overhydration effect was observed: all structural refinements at different pressures for both zeolites showed residual peaks lower than 1.2 $e^-/Å^3$, generally close to the Ba1 position (< 0.05 Å). At 2.85 GPa, OW1 and OW2 sites were fully occupied (Table 3), but no new sites were detected. We cannot

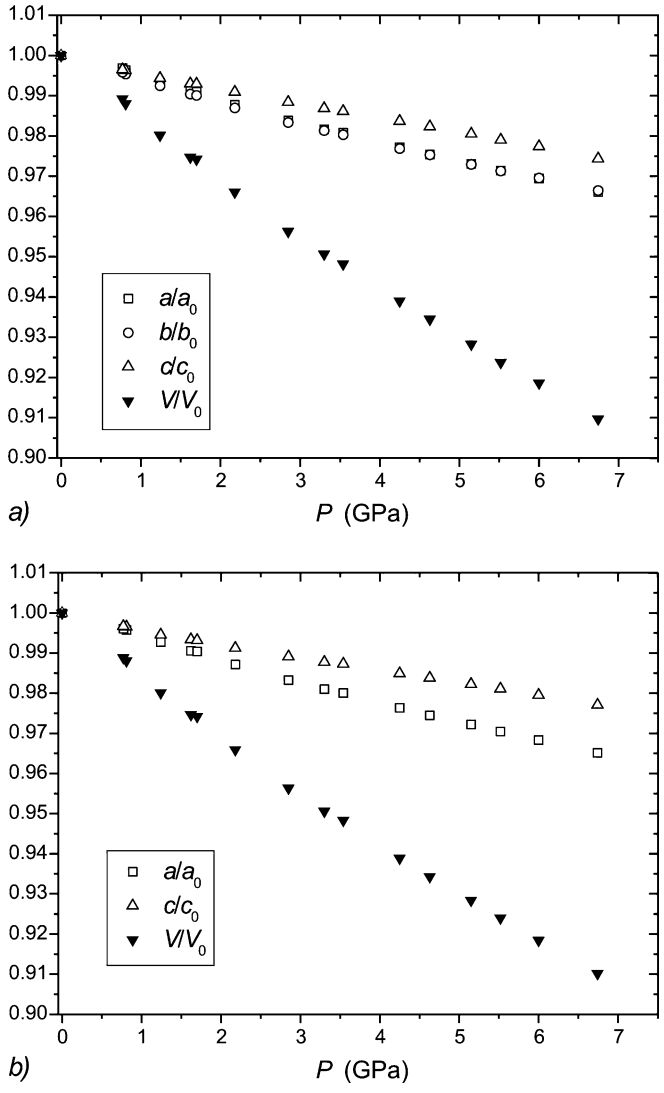

Fig. 2a,b Evolution with pressure of the unit-cell parameters of **(a)** orthorhombic and **(b)** tetragonal edingtonite, normalized with respect to the room pressure value. The esds values are smaller than the size of the symbols

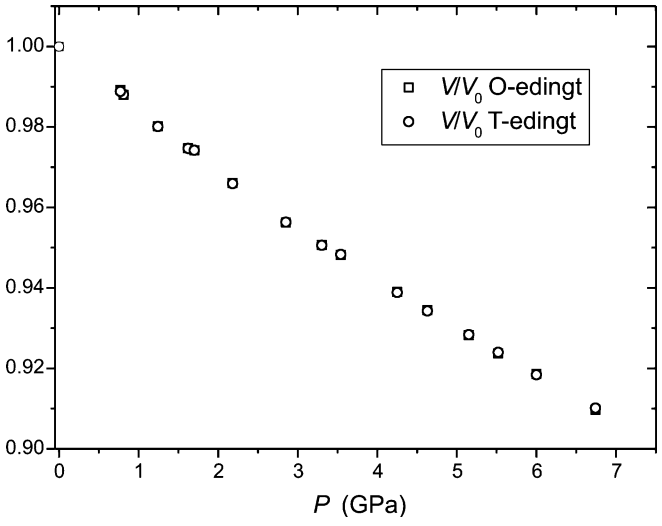

Fig. 3 Comparison between the cell volume behaviour of O- and T-edingtonite with pressure

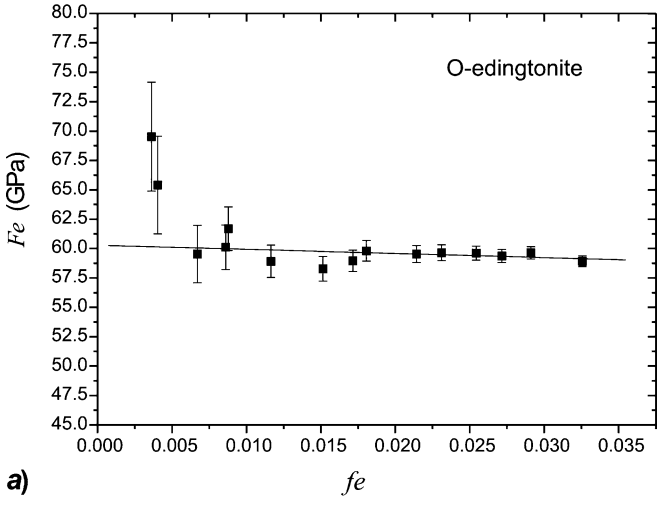

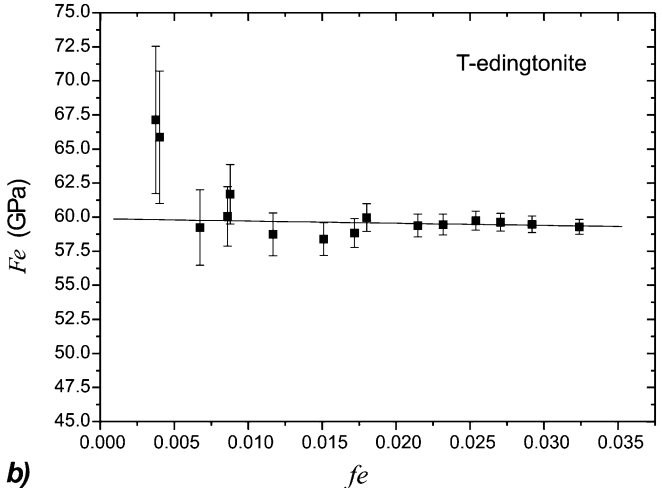

Fig. 4a,b Finite strain ($f_e = [(V_0/V)^{2/3} - 1]/2$) *vs.* the normalized stress ($F_e = P/[3f_e(1+2f_e)^{5/2}]$) plot for **(a)** orthorhombic and **(b)** tetragonal edingtonite. The esds have been calculated according to Heinz and Jeanloz (1984)

exclude that the penetration of water molecules happened already at room pressure when edingtonite was immersed into a hydrous medium. However, it is clear that such penetration does not affect the overall structure of edingtonite.

Discussion and conclusions

This study on the orthorhombic and tetragonal edingtonite under the same conditions, with nominally hydrous penetrating pressure medium, allows us to compare the elastic behaviour, the structural evolution and the role played by the tetrahedral Si/Al distribution at high pressure.

Orthorhombic and tetragonal edingtonite have the same bulk modulus within the standard deviation,

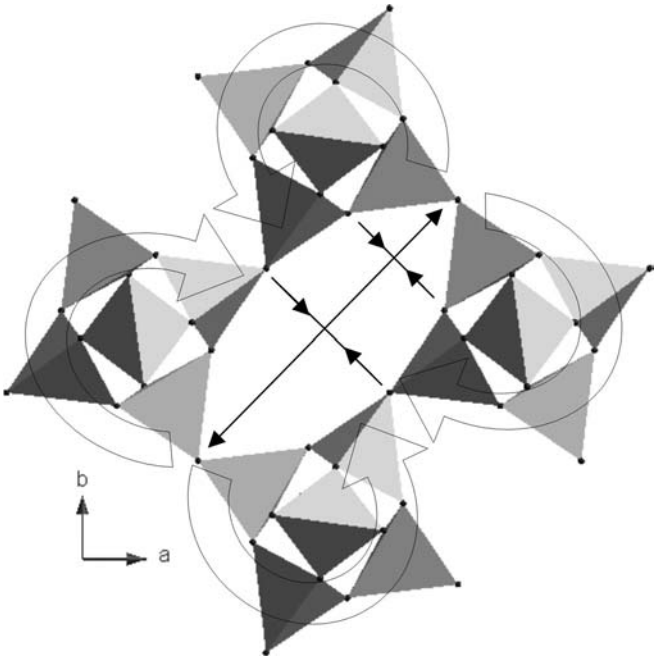

Fig. 5 SBU-cooperative rotation mechanism and relative effects on the [001]-channel free diameters at high-pressure

close to the value reported for the tetragonal edingtonite by Gatta et al. (2004) (BM-EoS: K_{T0} = 59(2) GPa – K = 3.4(8); K_{T0} = 57.9(6) GPa – K′ = 4), obtained using a non-penetrating anhydrous pressure medium. However, these results appear significantly lower than the value reported by Lee et al. (2004) (M-EoS: K_{T0} = 73(3) GPa – K′ = 4). Lee et al. (2004) showed two different bulk moduli (K_{T0} = 73(3) and K_{T0} = 68(2) GPa) obtained using two different V_0 values, measured under dry and under wet conditions, respectively. Refitting the volume data reported by Lee et al. (2004) with a second-order BM–EoS, excluding the V_0 value, gives the following EoS parameters: V_0 = 602(1) Å^3 and K_{T0} = 61(1) GPa (K = 4), in good agreement with the values of Gatta et al. (2004) and this study.

The bulk moduli obtained in this study for O- and T-edingtonite are slightly higher than the bulk moduli observed for other fibrous zeolites, such as scolecite (K_{T0} = 54.6(7) GPa – K′ = 4, Comodi et al. 2002) and natrolite (K_{T0} = 53(1) GPa – K′ = 4, before the phase transition at 1.5–2.0 GPa due to overhydration effects (Lee et al. 2002a).

The axial compressibilities show a pronounced anisotropy. On the other hand, the similar compressional pattern of the *a* and *b* axes for the O-edingtonite confirmed that the lattice behaviour of the fibrous zeolites is strongly controlled by the tetrahedral framework and by its topological symmetry (in this case tetragonal $P\bar{4}2_1m$) (Comodi et al. 2002; Gatta et al. 2003).

The structural evolution of the framework is characterized by one main deformation mechanism: the antirotation of the 4 = 1 SBU (Fig. 5), in agreement with the H*P* behaviour of other fibrous zeolites (Comodi et al. 2002; Gatta et al. 2003, 2004). This mechanism produces an axial compressibility strongly anisotropic (smaller along [001] than along [100] and [010]).

The compressional behaviour of the tetrahedral framework in O- and T-edingtonite, represented by SBU bulk moduli, was analyzed: the different Si/Al ordering slightly influences the elastic behaviour of the tetrahedral framework under H*P*-conditions, even though this effect is not evident on the lattice compressibility. The different SBU-volume variations with pressure, which lead to two different bulk modulus values (128(8) and 111(4) GPa for O- and T–edingtonite, respectively), are probably due to the different tetrahedral tilting: the angles Si1–O4–Al and Si1–O5–Si2 of the O-specimen (Fig. 1b) change from 138.41(9)0 to 134.66(10)^0 and from 141.83(7)^0 to 136.59(9)^0, respectively, in response to an applied pressure of 5.52 GPa (Table 5a), whereas in the same pressure range the angle T1–O45–T2 of the T-edingtonite (Fig. 1b) is reduced from 138.76(6)^0 to 135.27(11)^0 (Table 5b). The different tetrahedral tilting may also be responsible for the differences between the axial bulk moduli and their pressure derivatives for the *c* axis of O- and T-edingtonite.

The extra-framework content shows a similar evolution for both zeolites: the occupancy of the split Ba2 site decreases with increasing pressure and at 2.85 GPa this site is completely empty (Table 3). The reasons for this behaviour have been discussed by Gatta et al. (2004) and may be principally related to the reduction of the Ba–O bond distances at high pressure (Table 4), which leads to a new topological configuration energetically favourable with only one Ba site.

No penetration effect, leading to phase transformations, has been observed within the investigated pressure range, in spite of the hydrous pressure-transmitting medium used. However, the observed increasing of the occupancies of the water molecule sites (OW1, OW2) at high pressure is due to the penetrating effect of the pressure medium (Table 3). With respect to other zeolites, which show a dramatic penetrating effect of the pressure medium at relatively low pressures (Hazen and Finger 1984; Belitsky et al. 1992; Lee et al. 2002a, b), the extra-framework content of edingtonite fills a large amount of the channels free volume and hinders the mobility/penetration of new water molecules.

A comparison with the results obtained for T-edingtonite in glycerol (Gatta et al. 2004) shows that the high-pressure behaviour of edingtonite is quite independent of the medium used.

The crystal-structure modifications induced within the investigated pressure range are completely reversible for both specimens: the lattice parameters collected during decompression (Fig. 2; Table 1) are practically indistinguishable from those collected increasing pressure.

Acknowledgements Thanks are due to E. Galli (University of Modena, Italy) for the sample of edingtonite from Ice River and for the chemical analysis. Thanks to Yongjae Lee (Brookhaven National Laboratory, USA) for the pre-print of his paper. This work was financially supported by the Sofia Kovalevskaja Award to T. Boffa Ballaran. Comments by M. Gunter, S. Goryainov and Y. Seryotkin helped to improve the manuscript.

References

Allan DR, Miletich R, Angel RJ (1996) A diamond-anvil cell for single-crystal X-ray diffraction studies to pressures in excess of 10 GPa. Rev Sci Instrum 67:840–842

Amitin EB, Belitsky IA, Gabuda SP, Kovalevskaya YuA, Nabutovskaya OA, Polyanskaya TM (1981) Anomalies in the thermal expansion of edingtonite in the region of the structural phase transformations. J Struct Chem (RU) 22:441–442

Angel RJ (2000) Equation of state. In: Hazen RM, Downs RT (eds) High-temperature and high-pressure crystal chemistry. Reviews in Mineralogy and Geochemistry, vol. 41. Mineralogical Society of America and Geochemical Society, Washington, DC, pp 35–59

Angel RJ (2001) EOS-FIT V6.0. Computer program. Crystallography Laboratory, Dept. Geological Sciences, Virginia Tech, Blacksburg, USA

Angel RJ (2002) ABSORB V5.2. Computer program. Crystallography Laboratory, Dept. Geological Sciences, Virginia Tech, Blacksburg, USA

Angel RJ (2003a) Automated profile analysis for single-crystal diffraction data. J Appl Crystallogr 36:295–300

Angel RJ (2003b) WIN-INTEGRSTP V3.4. Computer program. Crystallography Laboratory, Dept. Geological Sciences, Virginia Tech, Blacksburg, USA

Angel RJ, Downs RT, Finger LW (2000) High-temperature – high-pressure diffractometry. In: Hazen RM, Downs RT (eds) High-temperature and high-pressure crystal chemistry. Reviews in Mineralogy and Geochemistry, vol. 41. Mineralogical Society of America and Geochemical Society, Washington, DC, pp 559–596

Armbruster T, Gunter ME (2001) Crystal structures of natural zeolites. In: Bish DL, Ming DW (eds) Natural zeolites: occurrence, properties, application. Reviews in Mineralogy and Geochemistry, vol. 45, Mineralogical Society of America and Geochemical Society, Washington, DC, pp 1–57

Baerlocher Ch, Meier WM, Olson DH (2001) Atlas of zeolite framework types, 5th edn, Elsevier, Amsterdam, NL, 302 pp

Ballone P, Quartieri S, Sani A, Vezzalini G (2002) High-pressure deformation mechanism in scolecite: a combined computational–experimental study. Am Mineral 87:1194–1206

Belitsky IA, Fursenko BA, Gabuda SP, Kholdeev OV, Seryotkin YV (1992) Structural transformation in natrolite and edingtonite. Phys Chem Miner 18: 497–505

Belitsky IA, Gabuda SP, Joswig W, Fuess H (1986) Study of the structure and dynamics of water in the zeolite edingtonite at low temperature by neutron diffraction and NMR-spectroscopy. N Jb Miner Mh 1986:541–551

Belitsky IA, Gabuda SP, Drebushchak VA, Naumov VN, Nogteva VV (1984) The specific heat of edingtonite at 5–316 K and the entropy and enthalpy under standard conditions. Geochem Int 21:21–23

Birch F (1947) Finite elastic strain of cubic crystal. Phys Rev 71:809–824

Burnham CW (1966) Computation of absorption corrections and the significance of end effects. Am Mineral 51:159–167

Comodi P, Gatta GD, Zanazzi PF (2002) High-pressure behaviour of scolecite. Eur J Mineral 14:567–574

Flack HD (1983) On enantiomorph-polarity estimation. Acta Crystallogr (A) 39:876–881

Galli E (1976) Crystal structure refinement of edingtonite. Acta Crystallogr (B)32:1623–1627

Gatta GD, Boffa Ballaran T (2004) New insight into the crystal structure of orthorhombic edingtonite. Min Mag (in press)

Gatta GD, Boffa Ballaran T, Comodi P, Zanazzi PF (2004) Isothermal equation of state and compressional behaviour of tetragonal edingtonite. Am Mineral (in press)

Gatta GD, Comodi P, Zanazzi PF (2003) New insights on high-pressure behaviour of microporous materials from X-ray single-crystal data. Micr Mesop Mat 61:105–115

Gatta GD, Boffa Ballaran T, Comodi P, Zanazzi PF (2004) Isothermal equation of state and compressional behaviour of tetragonal edingtonite. Am Mineral 89:633–639

Gottardi G, Galli E (1985) Natural zeolites, Springer, Hiedelberg, New York, 409 pp

Goryainov SV, Belitsky IA (1986) Analysis of vibrational spectra and phase transitions in zeolite (natrolite, edingtonite, chabasite). Proceedings 2nd International Conference Occurrence, Properties and Utilization of Natural Zeolites, Budapest, pp 257–264

Goryainov SV, Kursonov AV, Miroshnichenko YuM, Smirnov MB, Kabanov IS (2003) Low-temperature anomalies of infrared band intensities and high-pressure behaviour of edingtonite. Micr Mesop Mat 61:283–289

Hazen RM, Finger LW (1984) Compressibility of zeolite 4A is dependent on the molecular size of the hydrostatic pressure medium. J Appl Phys 56:1838–1840

Heinz DL, Jeanloz R (1984) The equation of state of the gold calibration standard. J Appl Phys 55:885–893

Ibers JA, Hamilton WC (eds) (1974) International tables for X-ray crystallography, vol. IV, Kynoch, Birmingham, UK

King HE, Finger LW (1979) Diffracted beam crystal centering and its application to high-pressure crystallography. J Appl Crystallogr 12:374–378

Kvick A, Smith JV (1983) A neutron diffraction study of the zeolite edingtonite. J Chem Phys 79:2356–2362

Lee Y, Vogt T, Hriljac JA, Parise JB, Artioli G (2002a) Pressure-induced volume expansion of zeolites in the natrolite family. J Am Chem Soc 124:5466–5475

Lee Y, Vogt T, Hriljac JA, Parise JB, Hanson JC, Kimk SJ (2002b) Non-framework cation migration and irreversible pressure-induced hydration in a zeolite. Nature 420:485–489

Lee Y, Hriljac JA, Studer A, Vogt T (2004) Anisotropic compression of edingtonite and thomsonite to 6 GPa at room temperature. Phys Chem Miner 31:22–27

Mao HK, Xu J, Bell PM (1986) Calibration of the ruby pressure gauge to 800 kbar under quasi-hydrostatic conditions. J Geophys Res 91:4673–4676

Mazzi F, Galli E, Gottardi G (1984) Crystal structure refinement of two tetragonal edingtonites. N Jb Miner Mh 1984:373–382

Miletich R, Allan DR, Kush WF (2000) High-pressure Single-Crystal Techniques. In: Hazen RM, Downs RT (eds) High-temperature and high-pressure crystal chemistry. Reviews in Mineralogy and Geochemistry, vol 41. Mineralogical society of America, Washington, DC, pp 445–519

Ralph RL, Finger LW (1982) A computer program for refinement of crystal orientation matrix and lattice constants from diffractometer data with lattice symmetry constraints. J Appl Crystallogr 15:537–539

Sheldrick GM (1997) SHELX-97. Programs for crystal structure determination and refinement. Institut für Anorg Chemie, Univ of Göttingen

Ståhl K (1998) In situ studies of the dehydration of edingtonite and brewsterite. Proc. 5th European Powder Diffraction Conference, Parma, Italy. Mat Science Forum. 278:666–671

Ståhl K, Hanson JC (1998) An in situ study of the edingtonite dehydration process from X-ray synchrotron powder diffraction. Eur J Mineral 10:221–228

Taylor WH, Jackson R (1933) The structure of edingtonite. Z Kristallogr 86:53–64

Van Reeuwijk LP (1972) High-temperature phases of zeolites of the natrolite group. Am Mineral 57:499–510

Van Reeuwijk LP (1974) The thermal dehydration of natural zeolites. Published PhD Thesis, Dissertation no. 587, Wageningen Universiteit, NL, 88 pp